The dependence of the rate of LiF ion pairing on the description of molecular interaction

Eva Pluhařová,[†] Marcel D. Baer,[¶] Gregory K. Schenter,[¶] Pavel Jungwirth,[†] and Christopher J. Mundy[*,¶]

Institute of Organic Chemistry and Biochemistry, Academy of Sciences of the Czech Republic, Flemingovo nam. 2, 16610 Prague 6, Czech Republic, Ecole Normale Superieure – PSL Research Univ., Chemistry Department, Sorbonne Universites-UPMC Univ. Paris 06, CNRS UMR 8640, 24 rue Lhomond, 75005 Paris, France, and Physical Sciences Division, Pacific Northwest National Laboratory, Richland, WA 99352

E-mail: chris.mundy@pnnl.gov

[*]To whom correspondence should be addressed

[†]Institute of Organic Chemistry and Biochemistry, Academy of Sciences of the Czech Republic, Flemingovo nam. 2, 16610 Prague 6, Czech Republic

[‡]Ecole Normale Superieure – PSL Research Univ., Chemistry Department, Sorbonne Universites-UPMC Univ. Paris 06, CNRS UMR 8640, 24 rue Lhomond, 75005 Paris, France

[¶]Physical Sciences Division, Pacific Northwest National Laboratory, Richland, WA 99352

Abstract

We present an analysis of the dynamics of ion-pairing of Lithium Fluoride (LiF) in aqueous solvent using both detailed molecular simulation as well as reduced models within a Generalized Langevin Equation (GLE) framework. We explored the sensitivity of the ion-pairing phenomena to the details of descriptions of molecular interaction, comparing two empirical potentials to explicit quantum based density functional theory. We find quantitative differences in the potentials of mean force for ion-pairing as well as time dependent frictions that lead to variations in the rate constant and reactive flux correlation functions. These details reflect differences in solvent response to ion-pairing between different representations of molecular interaction and influence anharmonicity of the dynamic response. We find that the short time anharmonic response is recovered with a GLE parameterization. Recovery of the details of long time response may require extensions to the reduced model. We show that the utility of using a reduced model leads to a straight forward application of variational transition state theory concepts to the condensed phase system. The significance of this is reflected in the analysis of committor distributions and the variation of planar hypersurfaces, leading to an improved understanding of factors that determine the rate of LiF ion-pairing.

Introduction

An improved understanding of both the simulation protocol for computing rates in the condensed phase and the underlying sensitivity of the reaction dynamics phenomena to the choice of the representation of molecular interaction remains an active area of research. In particular the connection between the microscopic descriptors, such as a potential of mean force (PMF), to the rates and mechanisms of nucleation[1–6] remain important concepts that connect the molecular and continuum theoretical frameworks. It has been long understood that the necessary ingredients for a reduced model based on a molecular description for condensed phase reactions rely on the knowledge of both PMF and the solvent friction along a prescribed reaction coordinate.[7–9] The PMF contains the thermodynamic information, and the friction allows for the coupling to the correlated solvent degrees of freedom yielding important dynamical effects (non-equilibrium solvent response).[8–10] The combination of a friction and PMF forms the foundation of a Generalized Langevin Equation (GLE). To date, there is a body of literature that utilizes model frictions and PMFs in conjunction with a GLE to study generic features of condensed phase dynamics and rates.[11–16] Important concepts as to the general form of a friction, namely its coordinate dependence, have been explored as extensions to GLEs where it is standard practice to consider only a single friction at the location of barriers.[11–13,17] However, to date there are few studies that have incorporated realistic frictions from a molecular simulation in conjunction with a PMF to examine the differences and similarities of an appropriately constructed reduced model to true dynamics of a full system.[17]

Herein, we present a detailed analysis of the dynamics of ion-pairing of lithium fluoride (LiF) that is implicated in the initial stages of nucleation. The particular choice of LiF was chosen in a previous study because of the tight solvation shells exhibited by Li^+ and F^- that are instead more amenable to the use of quantum based force fields using classical nuclei. In a recent study a direct comparison between Kohn-Sham density functional theory (DFT) and a variety of classical empirical interaction potentials revealed dramatic differences among these computational approaches in the PMF between the two ions in water as a function of there internuclear separation.[18] In particular, the barrier between solvent separated ion-pair (SSIP) and the contact ion-pair (CIP) is

significantly larger for DFT than that obtained with classical empirical potentials. Although there is no definitive experiment regarding the precise nature of the ion-paring of LiF, recent simulation studies regarding the hydration structure and ion-pairing in other electrolyte systems in conjunction with extended X-ray adsorption fine structure (EXAFS) studies suggest a picture where interaction potentials based in quantum mechanics have superior performance over their classical empirical counterparts (even when including dipole polarization) for the prediction of local solvation structure.[19–22] DFT takes into account the subtle balance between local water-water and ion-water interactions that becomes more significant as the symmetry of the homogeneous water system is broken by the present of ions. For a good description of the water-water interaction the use of the empirical dispersion correction introduced by Grimme[23] was shown to be necessary for the BLYP functional used here.[24]

Herein, we investigate the implications of different PMFs and the corresponding solvent friction kernels arising from different representations of molecular interaction on the rate of ion-pairing of LiF in the condensed phase. To this end we compare the reactive flux calculations of the full molecular system to the results from the construction of a reduced 1-dimensional model based on a GLE. In general, we find that the agreement between the two approaches is excellent. A further indication that the GLE contains the salient dynamical information is developed when examining the quality of the reaction coordinate through a committor analysis.[25,26] Recently, the subtleties of the committor analysis and its modifications were shown to be important when determining a transition state surface that maximizes the reactive flux.[26] The analysis presented here indicates that when the full dynamics is mapped to a 1-dimensional GLE, the maximization of the reactive flux can be efficiently obtained within in the framework of variational transition state theory (VTST).[27,28] Additionally, the comparison of the reactive flux utilizing the full PMF to harmonic approximations based on Grote-Hynes (GH) theory[8] are made. In this case, an improved estimate of the rate constant is obtained from VTST from rotating the dividing surface to include solvent bath coordinates. The results of our study suggest a picture that implicates the differences in the solvent response to the ion-pair due to different representations of interactions that is respon-

sible for the observed rates. The importance of these non-linearities in the ion-water interaction are viewed through the underlying dynamics yielding a clear picture of the dynamics of ion-pairing of LiF.

Methods

All of the details of the simulations performed with both classical and quantum-based interaction potentials herein are identical to those previously published where the equilibrium properties such as the PMF were compared and contrasted using different representations of the molecular interaction.[18] As was detailed in the aforementioned study there were significant differences in the PMF between empirical potentials and quantum based interaction potentials. The assumption that the fidelity of the ion-pair formation is well represented by DFT (BLYP functional[29,30] with Grimme correction scheme D2[23]) is based on the strong evidence of the ability of quantum based interaction potentials to quantitatively describe the experimentally determined hydration structure of a variety of simple and complex ions.[19–22] The parameterization of Dang and co-workers[31] in conjunction with SPC/E water[32] (Dang-SPC/E) provides the overall best agreement with the DFT ion pairing PMF. However, there remains some substantial differences between the two PMFs, most notably that the barrier to the CIP in the Dang-SPC/E study is significantly more shallow whereas DFT puts these two states roughly at the same free energies. Interestingly, the PMF that has the overall worst agreement with both the Dang-SPC/E and the DFT utilizes the OPLS force field[33] in conjunction with TIP4P[34] water (OPLS-TIP4P) where both the depth of the CIP and the barrier to the SSIP are distinct from the Dang-SPC/E and the DFT results.

Given the similarities and differences previously published and summarized above regarding the sensitivity of the equilibrium properties of ion-pairing to the interaction potential, it is natural to investigate and understand the consequences of these differences in the dynamical processes. To this end, we will investigate how the rate of ion-pair formation is influenced by both the PMF and the underlying relaxation process of the water bath. In order to ascertain the "correct" dynamics

for the LiF ion-pairing process the reactive flux method in conjunction with the full canonical sampling of the water/ion-pair system is employed. The rate going from A (the CIP state) to B (the SSIP) is k_{AB} is given by

$$Q_{\mathrm{R}} k_{\mathrm{AB}} = \lim_{t \to t_{\mathrm{plateau}}} Q \langle \frac{dq(0)}{dt} \delta[q(0)] \theta[q(t)] \rangle. \tag{1}$$

Here, Q_{R} is the reactant partition function, Q is the total partition function, $\delta(x)$ is the Dirac delta function, t_{plateau} is the plateau time when the rate is not a well defined exponential process, and $\theta(x)$ denotes the Heaviside step function that is 0 when $x < 0$ and 1 otherwise, and the coordinate q and its time derivative $\frac{dq}{dt}$ represent the position and velocity, respectively of the reactant species along the prescribed reaction coordinate. The $\lim_{t \to 0}$ limit of Eq. 1 defines the transition state theory (TST) rate that neglects all recrossings of the barrier and is thus an upper bound to the true rate constant. The exact rate is defined by $\kappa k_{\mathrm{AB}}^{\mathrm{TST}}$ where κ is the dimensionless recrossing factor defined as the ratio of the exact rate to the TST rate yielding,[35]

$$\kappa = \frac{\langle \frac{dq(0)}{dt} \delta[q(0)] \theta[q(t)] \rangle}{\langle \frac{dq(0)}{dt} \delta[q(0)] \theta[\frac{dq(0)}{dt}] \rangle}. \tag{2}$$

The classical molecular dynamics simulations with empirical interaction potentials were performed to compute the correlation function in Eq. 2 at constant volume with 3D periodic boundary conditions. The long-range electrostatic interactions were treated by the particle mesh Ewald method,[36] van der Waals and the short range electrostatic interactions were truncated at 0.6 nm. The geometry of water molecules was kept rigid using the Settle algorithm as implemented in GROMACS.[37] In the simulations from which the $F(t)$ was extracted constant temperature of 300 K was maintained by a CSVR thermostat[38] with a time constant of 0.5 ps. The trajectory of 1 ns length was collected using a leap-frog algorithm with a time-step of 0.5 fs while keeping the interionic distance fixed. 10000 initial configurations for the reactive flux trajectories were obtained using a sampling interval of 5 ps from an NVT simulation in which the interionic distance correspond to the transition state. After generating velocities corresponding to the distribution at

300 K, short 5 ps trajectories were collected by forwards and backwards propagation in time to make connections between the reactive flux obtained using the full dynamics and the harmonic approximation of GH theory.

Resampling in the vicinity of the barrier region for the DFT PMF shown in Fig. 1 was performed with the same DFT protocol as detailed in Ref. 18 and using the umbrella sampling protocol similar to that used in Ref. 39. Specifically, we performed sampling in 9 windows with a width of 0.1Å using harmonic constraint of the form $k(q-q_0)^2$ varying q_0 over $2.3-r^{\ddagger}$ to $3.0-r^{\ddagger}$ (see Tab. 1). The force constant k was set to 80 kJ/Å^2 for all windows. The bracketing windows at $2.3-r^{\ddagger}$ and $3.0-r^{\ddagger}$ were run for 7 ps of production. All intermediate windows were run a minimum of 20 ps. The free energy and error bars were computed using the Weighted Histogram Analysis Method (WHAM)[40] where the first 80 steps as a correlation time. Results are shown and discussed in Fig. 6.

Results and Discussion

The PMF and the harmonic fit to the transition state region are depicted in Fig. 1. Note that the anharmonic features in the DFT PMF have significant consequences on the dynamics and resulting rate constant and time dependencies of $\kappa(t)$. The effective barrier (imaginary) frequency is higher, driving the trajectories away from the barrier faster (this is counteracted by the larger friction of the DFT interaction potential). In addition the SSIP minimum is deeper, leading to reduced recrossing due to the interaction and anharmonicity, in contrast to the cases using classical empirical interaction potentials. Notice that the barrier for the SSIP to CIP motion (negative q direction) is comparable to $k_{\mathrm{B}}T$ for the classical interaction potentials. The recrossing factor, κ rate is generated using Eq. 2 by initializing ion-pair of the full condensed phase system by initiating microcanonical trajectories consistent with initial conditions generated by the canonical ensemble at the barrier region defined by $q=0$ in Fig. 1 separating the CIP from the SSIP. Similarly, we aim to construct high fidelity models of the full condensed phase system through a GLE by utilizing

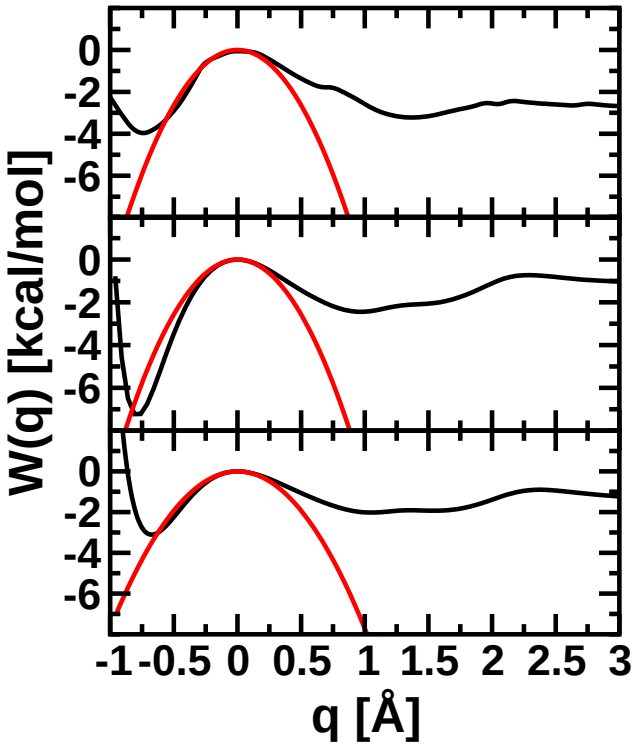

Figure 1: The Potential of mean force (black) and the harmonic fit to the transition state region (red) for DFT, OPLS-TIP4P and DANG-SPC/E from top to bottom.

the PMF along the prescribed coordinate in conjunction with a solvent friction comprising the bath degrees of freedom. The explicit form of GLE Hamilton can be written for a 1-dimensional reaction coordinate, q as

$$H = \frac{p^2}{2\mu} + W(q) + \sum_i \frac{P_i^2}{2m_{\mathrm{B}}} + \frac{m_{\mathrm{B}}}{2}(Q_i - c_i(q))\omega_i^2(Q_i - c_i(q)). \tag{3}$$

Here, $q = |\vec{\Delta r}| - r^{\ddagger} \equiv |\vec{r}_{\mathrm{Li}^+} - \vec{r}_{\mathrm{F}^-}| - r^{\ddagger}$, p is the momentum associated with the reacting particle with a reduced mass, μ, W is the PMF, P_i, Q_i, and ω_i denote the i-th bath momentum, position, and frequency with mass m_{B}. $r^{\ddagger}$ is the distance between the two ions at the barrier in order to enforce a barrier position $q = 0$ and are tabulated in Table 1. In general, $c_i(q)$ are the coefficients representing distance dependence friction, $\eta(t,q) = \beta\langle F_q(0)F_q(t)\rangle$ where $F_q(t)$ is the total force of the ion paring process projected along q, namely $\frac{1}{2}(\vec{F}_{\mathrm{Li}^+} - \vec{F}_{\mathrm{F}^-}) \cdot \frac{\vec{\Delta r}}{|\vec{\Delta r}|}$. The distance dependent

coefficients are determined through the relation

$$\frac{dc_i(q)}{dq} \equiv c_i'(q) = \int_0^{t_c} dt \cos(\omega_i t)\eta(t,q) \tag{4}$$

with the i-th frequency, ω_i is given by $(i-\frac{1}{2})\pi/t_c$.[14,41]

To make the connection to GH theory[8] and VTST,[42] it is instructive to diagonalize Eq. 3 in its fully linearized form. To this end, we write $V_{\rm tot} = W(q) + m_{\rm B}(\mathbf{Q}-\mathbf{c}(q))\cdot\omega^2\cdot(\mathbf{Q}-\mathbf{c}(q))/2$ to second order around the saddle point, $q^{\ddagger}=0$ where $\mathbf{c}=\{c_i\}, \mathbf{Q}=\{Q_i\}, \omega^2=\{\omega_i\}^2$, and $\mathbf{x}=\{q,Q_i\}$ as

$$V_{\rm tot} = \frac{m_{\rm B}}{2}\mathbf{x}\cdot\begin{pmatrix} \frac{\partial^2 V_{\rm tot}}{\partial q^2} & -\frac{\partial \mathbf{c}}{\partial q}\cdot\omega^2 \\ -\omega^2\cdot\frac{\partial \mathbf{c}}{\partial q} & \omega^2 \end{pmatrix}\cdot\mathbf{x} \tag{5}$$

where we notice that the first order term in $W(q)$ vanishes at the saddle point, and $\mathbf{Q}_{\rm bath}\equiv\mathbf{Q}-\mathbf{c}(q)$, and $\partial^2 V_{\rm tot}/\partial q^2 = \partial^2 W(q)/\partial q^2 + m_{\rm b}(\partial\mathbf{c}/\partial q\cdot\omega^2\cdot\partial\mathbf{c}/\partial q + \mathbf{Q}_{\rm bath}\cdot\omega^2\cdot\partial^2\mathbf{c}/\partial^2 q)$.

An important ingredient to performing the GLE dynamics in Eq.(3) is to establish an adequate representation of the bath degrees of freedom. In this study we choose $t_c = 8$ps in conjunction with 100 cosine functions. The distance dependent dependence of c_i' is determined by sampling the solvent friction, $\eta(t,q)$ along the reaction coordinate sampled at 0.1Å. All numerical quantities, namely $W(q)$ and $c_i'(q)$ were represented by splines. The determination of $c_i(q)$ from $c_i'(q)$ was performed by analytically integrating the splined polynomial piecewise over the appropriate interval. A representative set of frictions for each description of the interaction is given in Fig. 2. There is excellent agreement of representation the representation of the bath between the full condensed phase simulation and the cosine fit. Thus, a robust, energy conserving protocol is obtained for simulating a 1-dimensional system given by Eq. (3).

One of the purposes of this study is to establish consistency in the rate of ion pairing as determined by the reactive flux in Eq. (1) using the full potential and the dynamics obtained by the construction of the reduced 1-dimensional model in the form of a GLE for a variety of forms of interaction. Here we present the results of the rate of ion-paring as determined by two differ-

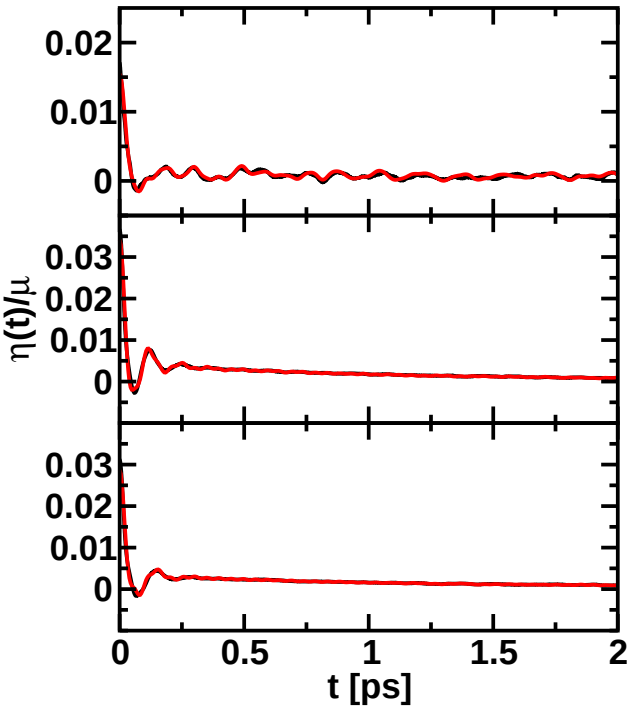

Figure 2: Comparison of friction at q=0 (black) and the cosine fit (red) for DFT, OPLS, DANG-SPC/E cases respectively (top to bottom).

ent classical empirical interaction potentials, OPLS-TIP4P (OPLS[33] parameterization for the ions and TIP4P[34] water) and Dang-SPC/E (Dang and co-workers[31] parameterization for the ions and SPC/E[32] water). Additionally, we can examine the consequences on computing the recrossing factor using GH theory with a single friction at the transition state to the use of the full PMF using both a single friction and coordinate dependent friction. The reader is reminded that within GH theory the recrossing factor is given by the self-consistent solution to

$$\kappa_{\rm GH} = [\kappa_{\rm GH} + \int_0^\infty dt \frac{\eta(t,q^\ddagger)}{\mu\,\omega^\ddagger} \exp(t\,\kappa_{\rm GH}\omega^\ddagger)]^{-1} \tag{6}$$

where $\kappa_{\rm GH}$ is the GH recrossing factor, $q^\ddagger = 0$ represents the position of the transition state, and $\omega^\ddagger$ is the frequency of the barrier as determined by a fit to a harmonic potential.[8] The salient feature of using Eq. (6) is that under a suitable representation of the solvent friction and PMF one does not need to perform the averages in Eq. 2 using the full condensed phase system. Rather, based on a single calculation of the solvent friction at the barrier and a harmonic fit to the PMF in the

barrier region to obtain $\omega^{\ddagger}$, the recrossing factor is a simple iterative solution to Eq. 6. There is

Table 1: Table of parameters used in GH theory.

Model	$r^{\ddagger}$[Å]	$\omega^{\ddagger}$[cm^{-1}]	κ_{GH}
DFT	2.6142	221.06	0.572
OPLS-TIP4P	2.7098	218.28	0.298
DANG-SPCE	2.9818	189.12	0.258

strong evidence in the literature that the GH theory works quite well for the ion pairing of NaCl.[43] A recent study of the pressure dependence of the water exchange around a Li^+ ion found that the rates for water exchange computed with Eq. 2 using the full potential did not agree with the GH recrossing factor.[44] As can be seen herein, the recrossing factor from the dynamics utilizing the full potential for LiF ion pairing is distinct from that obtained using the GH approximation. Here we wish to identify features in both the PMF and the solvent friction that give rise to differences in the recrossing factors for the specific case of LiF.

To this end, in an earlier study focusing on understanding rates of reactions on model systems, deviations from GH theory were also observed in systems that exhibited a "slow" friction bath, namely a spectral density of the representation of the bath that is dominated by low frequency modes.[14,41] Upon examination of the spectral density of the representation of the bath in the present study, it is found that it is indeed dominated by a large populations at low frequency. Moreover, a closer look at the Laplace transform of the friction suggests a significantly stronger coupling to the barrier frequency for the ion-paring using classical based interaction potentials. This brings up an interesting question of whether the low coupling to the barrier frequency as predicted using the DFT interaction potential produces a signature of the fundamental differences between the classical interactions in the short-range response.[45] Thus, our aim is to systematically study the quantitative differences between the full dynamics and its coarse grained representation to examine both effects of the anharmonicity of the PMF and representations of the solvent friction on the recrossing factor.

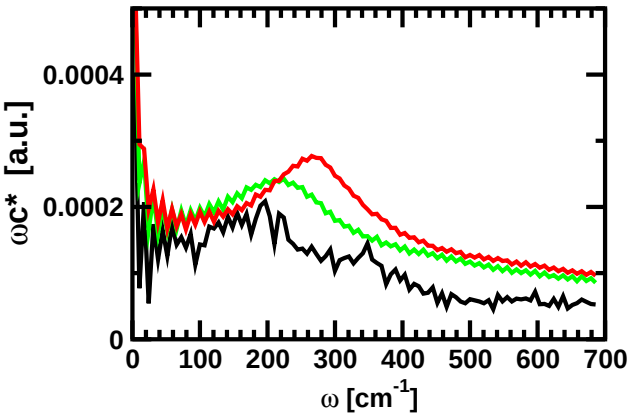

Figure 3: Comparison of spectral densities, DFT (blue), OPLS (green), and DANG-SPC/E (red).

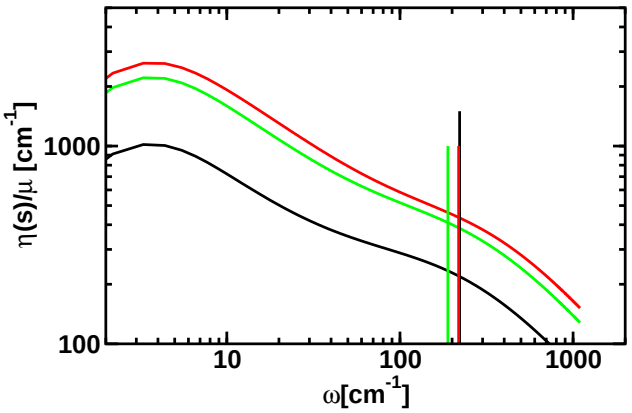

Figure 4: Laplace transform of friction for DFT (black), OPLS (red), and DANG-SPC/E (green). Impulse lines indicate the barrier frequency for each of the cases.

As pointed out above, the most general form of the solvent friction is obtained by bilinear coupling to the coefficients that determine the coordinate dependent friction through Eq. 4. Here we utilize both the solvent friction $c_i(q)$ and the more common linearization, namely $c_i'(q) \rightarrow c_i^* q$, where c_i^* is a constant representation of the bath that is fit to a friction at the transition state, $\eta(t, q^{\ddagger})$.

One of the main results of this study is shown in Fig. 5. Here we compare the recrossing factor using Eq. 2 with different representations of the solvent friction using the 1-dimension GLE to the results obtained with the full dynamical system using the classical empirical interaction potentials. As can be seen, The short-time dynamics, namely $t < t_{\text{plateau}}$ is nearly indistinguishable between the full dynamics and the 1-dimensional GLE. Although the results are not quantitative, at long-times the dynamics of the full system and the 1-dimensional GLE are in good agreement. It is a useful exercise to compare the value of the recrossing factor as obtained from Eq. (6) and tabulated in Table 1 to the results obtained from the calculation of the recrossing factor using harmonic fit to PMF, a solvent friction represented by c_i^*, and the 1-dimensional GLE. As expected, near quantitative agreement between the two results is obtained yielding a self-consistent check of our GLE implementation and confirming that GH theory for a harmonic system is indeed exact. One immediate insight that is gleaned is that the recrossing factor as determined by GH theory is significantly different than the recrossing factor computed using the full system for both classical models. Although there have been reported cases where GH both agree with and significantly deviate from the result of the reactive flux using the full potential the reasons as to why remain incomplete.[15,26,46]

In an attempt to obtain quantitative agreement between the reactive flux calculations of the full and reduced system we follow a recent study where it was shown that it was imperative to introduce a coordinate independent friction in order to fully reproduce the dynamics of hydrophobic assembly using a Brownian dynamics.[17] To this end we perform the reactive flux calculations using the full PMF in conjunction with $c_i(q)$ determined from Eq. 4. Surprisingly, the results in Fig. 5 suggest that there is no significant improvement over the use of a single friction on the agreement between the full and the reduced 1-dimensional model for ion-pairing. The insensitiv-

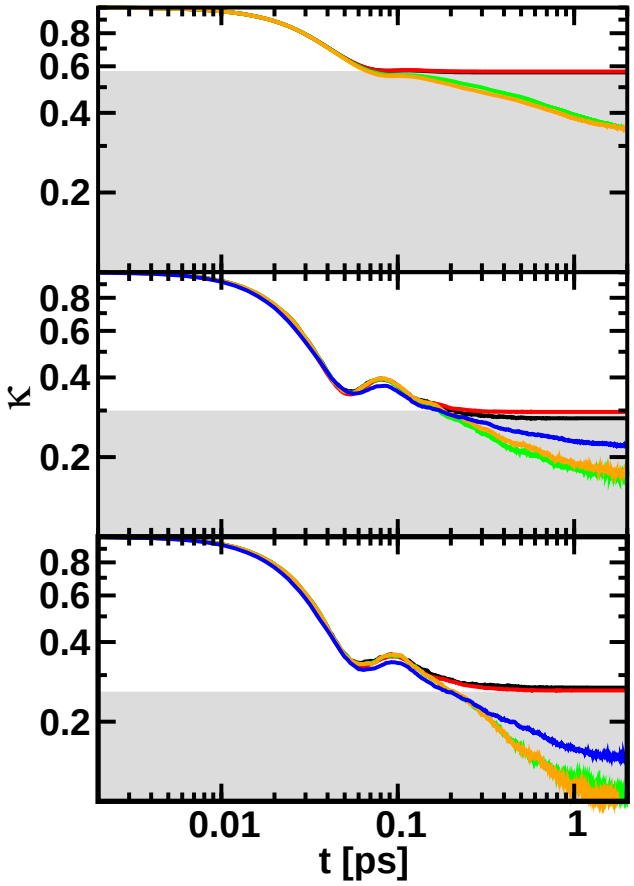

Figure 5: Comparison of recrossing factors correlation function versus time for the three cases, DFT, OPLS and DANG-SPC/E from top to bottom. Blue curves are the results from the simulation of the full, multidimensional system. Remaining curves represent results from the GLE simulation. Red curves represent harmonic, fixed-friction cases, while black curves represent harmonic, coordinate-dependent friction cases. Orange curves represent the anharmonic coordinate-dependent friction cases and green curves represent anharmonic fixed-friction cases. The border of the shaded grey area denotes the GH theory value as shown in Table 1.

ity to the description of the friction indicates that indeed the non-linearities in the underlying PMF play a dominant role. However, given that the non-equilibrium solvent effects are represented by a bilinear coupling to a bath, we believe that the agreement between the full and reduced system is nevertheless remarkable.

Given the reasonable agreement with the reactive flux calculations of the full system with those using the full PMF and coordinate dependent friction utilizing Eq. (3) we model the recrossing factor utilizing the PMF and frictions obtained from DFT calculations of the ion-pairing process in LiF. The results of the DFT reactive flux calculation are distinct from the OPLS-TIP4P and Dang-SPC/E results and show striking distinctions in the short-time dynamics. These differences are likely because of the weaker coupling of the DFT obtained friction to the barrier frequency as was discussed previously in Fig. 4.

Given the start contrast of the lower coupling to the barrier and the significantly higher recrossing factor, we provide a self-consistent check on the height and shape of the barrier of the DFT PMF using umbrella sampling. The consequences of a different shape of a barrier could have profound implications on the rate of ion-pairing. To this end, as detailed above, we resampled the barrier region of the Li-F PMF using the same DFT protocol as in Ref. 18 but with the umbrella sampling protocol that we have shown to converge quickly in regions with sharp gradients. The results are shown in Fig. 6. The results suggest that the PMF in the previous study is in excellent agreement with the PMF obtained using umbrella sampling. Given that any errors in the barrier width and height are unlikely, the present results suggest that it is indeed the anharmonicity of the PMF in conjunction with a "slow" bath as shown in Fig. 3 and the small coupling to the bath coordinate dipicted in Fig. 4 that is responsible for our significantly larger recrossing factor for the DFT case. Moreover, the anharmonicity of the underlying PMF seems to be the dominant effect over using the more realistic coordinate dependent friction to describe the bath. This, we believe, constitutes an explanation of deviations from GH theory for the case of LiF ion pairing.

Last we examine the protocol for determining the precise mechanism of ion-pairing using the 1-dimensional GLE formalism for modeling the full condensed phase dynamics. Here, we adopt

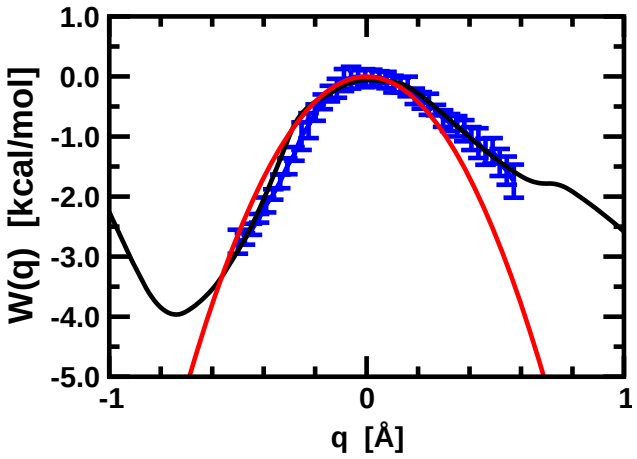

Figure 6: Resampled barrier region of the Li-F PMF (black) using the same DFT protocol as in Ref. 18 but with the umbrella sampling protocol (blue) and the harmonic fit to the transition state region (red).

the formalism that has been developed through transition path sampling (TPS) and the concept of a committor distribution and transition state ensemble (TSE).[25,26] The discussion of committor distributions and the TPE in conjunction with the ion-pairing of NaCl was first discussed by Geissler and co-workers.[46] In this study the authors demonstrated that the rate can be computed using the formulation of TPS. It is known that applying the techniques of VTST to problems in the condensed phase is doable but difficult.[47] The issues that plague VTST in the condensed phase, namely complex multidimensional minimum (free) energy searches, are overcome by using the TPS approach. Following definitions put forth by Truhlar and Garrett[15] we define the committor as

$$P_{\mathrm{B}}(r^*,Z) = \int h_{\mathrm{B}}\left[r(t_s;r^*,Z)\right] P_{\mathrm{T}}(p_r)dp_r. \tag{7}$$

Here, $P_{\mathrm{B}}(r^*,Z)$ is the probability that when a trajectory is started at position, r^* with bath coordinates $Z \equiv \{Q_i,P_i\}$, that after a trajectory length, t_s of 10 ps, the final state is in the product state B averaged over a the solute momenta, p_r that are thermally distributed over $P_{\mathrm{T}}(p_r)$. $h_{\mathrm{B}} = 1$ if the trajectory ends in the product region B after trajectory length t_s and is zero otherwise. In practice, one computes $P_{\mathrm{B}}(r^*,Z)$ using 50 to 100 trajectories using the 10 ps trajectories used to compute the recrossing factor where $P_{\mathrm{T}}(p_r)$ follows the standard Boltzmann distribution for the solute velocity cite,[25] namely $\int h_{\mathrm{B}}\left[r(t_s;r^*,Z)\right] P_{\mathrm{T}}(p_r)dp_r = 1/N\sum_i^N h_{\mathrm{B}}\left[r(t_s;r^*,Z)\right]$. Importantly, the distribution

of P_{B} is given by

$$P(P_{\mathrm{B}}) = \int \delta(P_{\mathrm{B}}^{*} - P_{\mathrm{B}}(r^{*}, Z)) P_{\mathrm{Z}}(Z) dZ. \tag{8}$$

Here δ denotes a delta-functional and $P_{\mathrm{Z}}(Z)$ is sampled over suitably chosen bath distribution. Eq. 8 is known as the committor distribution function in applications of TPS to rate theory.[15,26] A typical committor distribution function for our GLE dynamics is depicted in Fig. 7 using the construction of the PMF based on the distance between the Li^{+} and F^{-} as the reaction coordinate with barrier $q^{\ddagger}$ as shown in Fig. 1. The result in Fig. 7 is not surprising, and has been studied discussed by many researchers.[15,26,46] It is also another indication of the fidelity of our reduced GLE model. It was first pointed out by Peters[48] that a dividing surface obtained from a straightforward optimization of the committor distribution does not yield a recrossing factor of unity. Moreover, as also pointed out by Peters[26] modifications to optimizing the committor distribution based on concepts such as likelihood maximization also do not lead to unit recrossing factors.[16] Some small improvements to the recrossing factor can be made with the inertial likelihood maximization procedure.[16,26]

We take a slightly different approach to this problem, namely directly maximizing the reactive flux. Given that we have a satisfactory 1-dimensional GLE representation of the dynamics, all of the tools of VTST and GH theory can be straightforwardly implemented to define an optimal dividing surface or transition state. To this end, a diagonalization of Eq. 5 to yield

$$\begin{pmatrix} \frac{\partial^2 V_{\mathrm{tot}}}{\partial q^2} & -\frac{\partial \mathbf{c}}{\partial q} \cdot \boldsymbol{\omega}^2 \\ -\boldsymbol{\omega}^2 \cdot \frac{\partial \mathbf{c}}{\partial q} & \boldsymbol{\omega}^2 \end{pmatrix} \mathbf{U} = \mathbf{U}\boldsymbol{\lambda}^2 \tag{9}$$

where the eigenfrequency matrix $\boldsymbol{\lambda}^2$ is diagonal and the transformation matrices satisfy $\mathbf{U}^T\mathbf{U} = 1$. Based on a harmonic representation of the dynamics, we can find a rotated dividing surface defined by,

$$y_1 = \sum_{i=1}^{n} U_{i,1} q_i + \sum_{j=1}^{N} U_{(j+n),1} Q_j \tag{10}$$

where the first eigenvector corresponds to the reactive mode, $\lambda^2 < 0$. Initiating dynamics off of

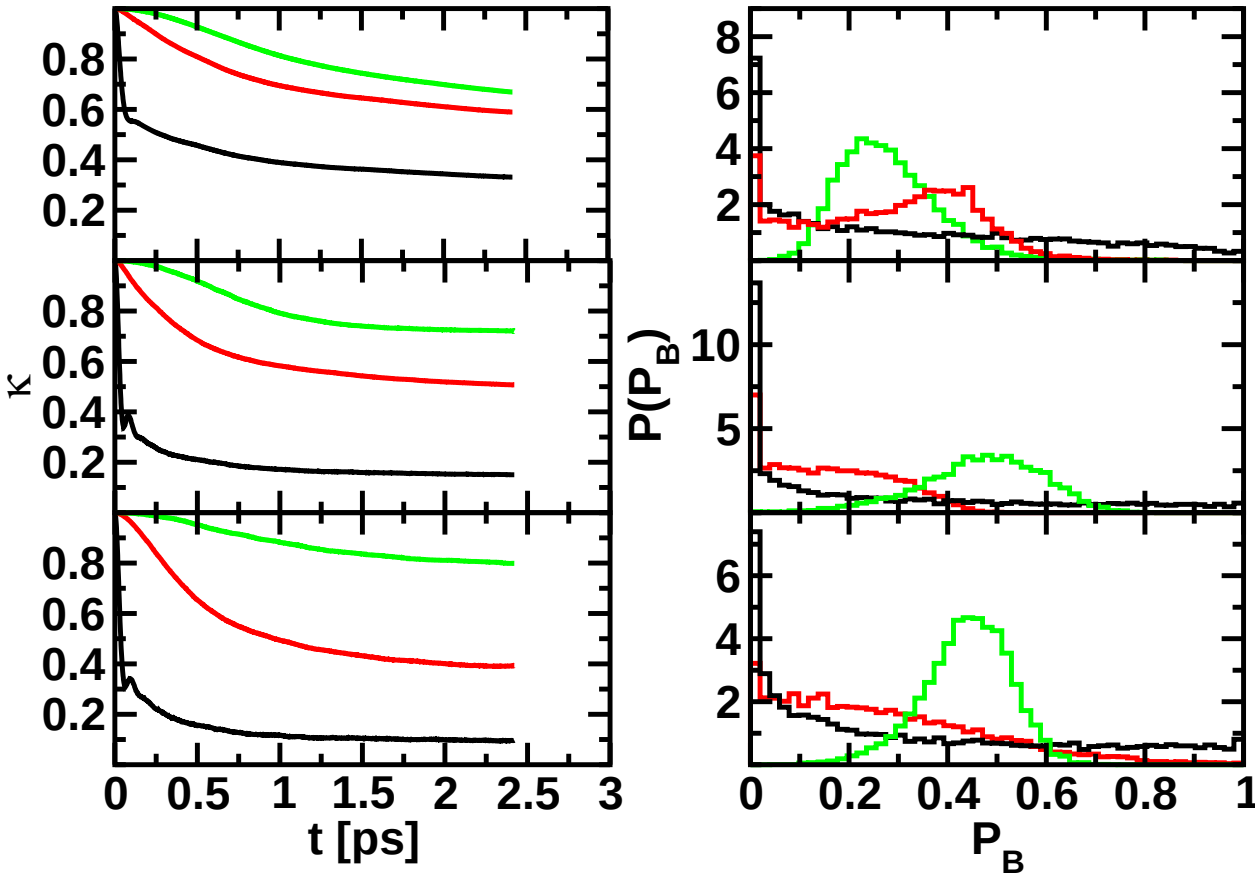

Figure 7: Comparison of the dynamic recrossing factor, $\kappa(t)$ (left frames), and the committor distribution $P(P_B)$ (right frames) for the three cases of dividing surfaces where trajectories are launched: 1) (black) the conventional TST q=0 dividing surface (hypersurface, TST of Figure 9). 2) (red) the $y_1 = 0$ dividing surface, the hypersurface perpendicular to the MEP at the saddle point, s=0. A harmonic TST analysis with this hypersurface corresponds to the Grote-Hynes estimate of the rate constant (hypersurface, GH of Figure 9). 3) (green) The variationally optimized hypersurface dividing surface corresponding to the maximum of the free energy of Figure 8. In this case, $s \neq 0$. (This is the VTST hypersurface of Figure 9) From top to bottom, we consider the three cases: A) DFT, B) OPLS, and C) DANG-SPC/E.

the hyper-surface defined by $y_1 = 0$ and accumulating the averages in Eq. 2 yields a significantly larger recrossing factors for all interaction potentials considered herein as depicted in Fig. 7. One can then accumulate the committor distribution functions defined in Eq. 8 which are again shown in Fig. 7. One sees that that indeed, rotating the diving surface from $q = 0$ to $y_1 = 0$ using a harmonic reference system provides a better approximation to true dividing surface as can be seen by both the committor distribution and the greatly improved (by more than a factor of two) reactive flux. Although we have demonstrated that the reactive flux can be greatly improved by rotating the dividing surface corresponding to that determined by a harmonic reference, the overall improvement of the committor distribution is not satisfactory. One can further improve on the maximization of the reactive flux by using the tools of VTST.

For this problem it is instructive to consider a sequence of hyperplane dividing surfaces, taking advantage of VTST. Such an approach, pioneered by Garrett and Truhlar,[27,28] has proven to be effective at extracting the essential features of the underlying dynamics that determine the rate constant, without performing any explicit dynamics. The approach has proven to be effective, describing both small molecule reactions as well as system-bath systems represented by a GLE.[10,14,15,41,49] For the current case, we consider the minimum energy path (MEP) of the full system-bath system. In a procedure that is consistent with the Miller, Handy and Adams[50] construction of the reaction path Hamiltonian, we follow the minimum energy path from the saddle-point of the full system, evaluating normal modes along the path, projecting out the motion along the MEP. A dividing surface for each value of the progress along the MEP, denoted s, is a hyperplane defined by the subspace of modes transverse to the motion along the MEP. A transition state estimate for the rate constant within a harmonic approximation is readily obtained as a function of s,

$$Q_R k^{\mathrm{TST}}(s) = \frac{k_{\mathrm{B}}T}{h} e^{-\frac{G^{\mathrm{TST}}(s)}{k_{\mathrm{B}}T}} \tag{11}$$

where $G^{\mathrm{TST}}(s)$ is the free-energy evaluated within a harmonic approximation. Such an approach is implemented in the POLYRATE computer program.[42] In Fig. 8 we display the evaluated $G^{\mathrm{TST}}(s)$ for all three cases of the representation of molecular interaction considered herein. Note that a

maximum of this curve corresponds to the best VTST estimate of the rate constant within the harmonic approximation.

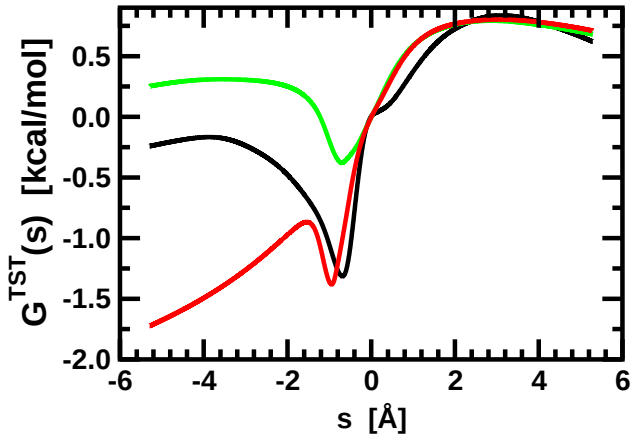

Figure 8: Variational transition state theory free energy as a function of reaction path parameter (s). (black) is DFT, (red) is OPLS, and (green) is DANG-SPC/E

It is instructive to examine three dividing surfaces (see Fig. 9). The first, corresponds to the surface defined by $q = 0$, a hyperplane that encompasses the bath degrees of freedom only. The estimate of the rate constant corresponding to this dividing surface is the "gas phase" (no-coupling to the bath) TST rate constant, and is our reference for κ with the exact rate being defined by $\kappa k^{\mathrm{TST}}(q = 0)))$. The harmonic TST estimate for the rate constant corresponding to the dividing surface at $s = 0$, containing the conventional saddle point, is equivalent to the GH estimate of the rate constant. This is the second dividing surface. The third dividing surface corresponds to the best harmonic VTST estimate of the rate constant, away from $q = 0$, corresponding to the maximum of $G^{\mathrm{TST}}(s)$. One would expect that an improved harmonic VTST estimate of the rate constant will lead to a larger plateau value for κ. In Fig. 7 we evaluate $\kappa(t)$ corresponding to the aforementioned three dividing surfaces. The exact rate constant, is the same for all three cases through the definition of $\kappa(t)$. It is remarkable how much of an improvement in the rate constant estimate is recovered by simply rotating the dividing surface to include bath degrees of freedom. ($q = 0$ vs. the $s = 0$ GH surface) Further improvement in the estimate of the rate constant is obtained by moving the hypersurface dividing surface away from the $q = 0$ saddle point. Although, we only see a small improvement in the reactive flux from the $s = 0$ surface to the VTST surface, the

committor distribution has greatly improved for the VTST surface and is centered around $P_B \sim \frac{1}{2}$ indicating that the VTST surface is an excellent candidate for a transition state.

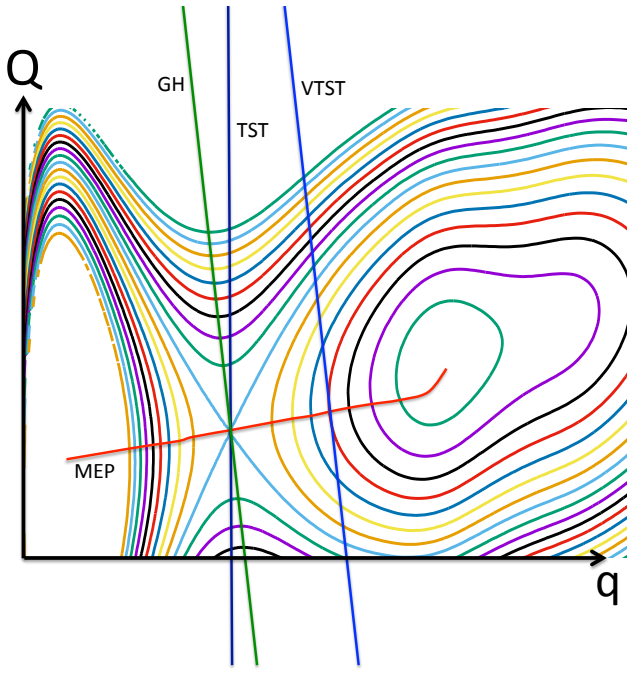

Figure 9: An illustration of the three dividing surfaces used in the analysis. The background contours represent the multidimensional potential energy surface in terms of the system coordinate, q, and the bath coordinate Q. MEP represents the multidimensional minimum energy path that starts in the reactant minimum, $s < 0$, passes through the saddle point, $s = 0$, and proceeds to the product minimum, $s > 0$. The three lines represent the three hypersurface dividing surfaces. TST is the conventional TST, $q = 0$, surface. GH is the hypersurface that is orthogonal to the reactive direction, corresponding to a Grote-Hynes estimate of the rate constant. VTST is the hypersurface that corresponds to the variationally optimized harmonic transition state theory rate constant.

Once a transition state surface candidate has been identified, the question as to the mechanism of the ion-pairing process can be addressed. However, the use of the 1-dimensional GLE does not easily lend itself to a molecular interpretation of the solvent reorganization leading to the ion-pairing process. Instead, we have access to the important frequencies that contribute to the ion-pairing process, but there is no clear one-to-one mapping between a particular frequency and a molecular picture. The frequency picture is further confounded when noticing the spectral density of the bath spans a significant frequency range. Specifically, in the limit of an adiabatic bath and the slow Kramers limit is represented throughout the minimum energy path that was constructed with the VTST analysis. Future work will be focused on making the connections of bath modes to

the microscopic descriptors that have recently been put forth regarding the rate of ion-pairing for a variety of salts.[51]

Conclusion

Herein, we have presented a formalism to construct a reduced model of the ion-pairing process through the computation of a PMF and the concomitant solvent friction. The aforementioned ingredients have long been known to form the basis of rate theory in the condensed phase.[7] Our findings suggest that it is possible to map the full 3N-dimensional problem to a 1-dimensional reaction coordinate coupled to a bath of 100 oscillators within the GLE framework. The fidelity of the dynamics of the GLE was shown to be generally good although fully quantitative agreement between the full system and the reduced model was never accomplished. Using a coordinate dependent friction, although giving some improvement in the quality of the dynamics did not provide a direct route to quantitative agreement. Nevertheless, quantitative agreement was achieved between the full system and the GLE for the reactive flux using GH theory.

A motivation for constructing a reduced model of the dynamics is that although the efficiency of DFT methods has allowed for the accurate determination of the PMF of ion-pairing[18] the ability to perform reactive flux dynamics and to converge a recrossing factor is still currently out of reach. Additionally, under the reasonable assumption that the DFT can converge a solvent friction on a 50 ps time scale, we then have the ability to directly compare the converged GLE dynamics using different representation of the interaction. The results, herein, suggest that the solvent friction and short-time dynamics show interesting differences between the DFT and the classical interaction potentials. Specifically, the weaker coupling of the DFT system in the barrier region is an interesting aspect of our findings that needs to be further explored. Specifically, the classical models considered in this research reflect a class of so-called frustrated charge models of water.[45] These models have a highly tuned balance between strong electrostatic attraction and Lennard-Jones repulsion that are known to accurately describe hydrogen bonding in the bulk in addition to the

long-range dielectric response. Signatures of the break down of these classical frustrated charge models for water under the inhomogeneous condition of the solvation of ions could be manifest in the weaker coupling of the solvent in the DFT picture to the high-frequency modes in the vicinity of the transition state as seen in Figs. 3 and 4. Moreover, the flexibility in the solvent response has also been found in other DFT studies of solvation.[52,53] We will continue to test and validate the aforementioned concepts on more well characterized systems, such as NaCl where there is a consensus in the literature on transition states and rates that have been studied with a variety of classical simulation protocols.[26,43,46,51,54]

Moreover, once a reduced dynamical model has been established interesting connections to committor distributions that define transition state ensembles can be made through the harmonic reference of GH theory and further corrections through VTST. Although the ideas of GH theory and VTST have been around for decades, the connections of these ideas to reactions in the condensed phase have not been fully exploited thus far. It is clear from this study, that the construction of a meaningful reduced model of reactions in the condensed phase through a PMF and friction is a viable way to connect the frameworks of GH theory and VTST. Moreover, our results suggest that indeed the harmonic system provides a good reference to maximize the reactive flux, producing a committor distribution function consistent with the concept of a transition state. Although the committor distribution does correlate with a maximum reactive flux, our study corroborates findings of Peters[26] that other more sophisticated definitions of the committor, such as inertial likelihood maximization, are needed to maximize the reactive flux. Nevertheless, it is important to point out that the framework of TPS is best suited as an unbiased protocol for determining mechanisms of reactions in full condensed phase simulations. However, computing rates though the TPS machinery is still much more involved than the straightforward reactive flux approach. What was demonstrated herein, is that the construction of the reduced model for a process in the condensed phase is a direct avenue for connecting *all* of the frameworks that have been developed for rate theory. Although the direct description of molecular detail cannot be ascertained within the GLE formulation, our future research directions are aimed at finding connections between the molecular

scale detail in a full simulation to the information present in the formulation of the bath coordinates. Importantly, the research presented herein is a way to utilize the information obtained from *ab initio* dynamics to compute converged rates providing important insights into how the inclusion of electronic structure modifies our understanding of chemical reactions in the condensed phase.

Acknowledgement

CJM and GKS are supported by the U.S. Department of Energy's (DOE) Office of Basic Energy Sciences, Division of Chemical Sciences, Geosciences and Biosciences. Pacific Northwest National Laboratory (PNNL) is operated for the Department of Energy by Battelle. MDB is grateful for the support of Laboratory Directed Research and Development funding under the auspices of PNNL's Laboratory Initiative Materials Synthesis and Simulation across Scales (MS^3). Additional computing resources were generously allocated by PNNL's Institutional Computing program. EP acknowledges support from PNNL's Alternate Sponsored Fellowship program and IMPRS Dresden.Support to P.J. from the Czech Science Foundation (grant P208/12/G016) and the Academy of Sciences (Praemium Academie award) is gratefully acknowledged.

References

(1) Schenter, G. K.; Kathmann, S. M.; Garrett, B. C. *Phys. Rev. Lett.* **1999**, *82*, 3484–3487.

(2) Kathmann, S. M.; Schenter, G. K.; Garrett, B. C. *Phys. Rev. Lett.* **2005**, *94*, 116104.

(3) Beckham, G. T.; Peters, B. *J. Phys. Chem. Lett.* **2011**, *2*, 1133–1138.

(4) Knott, B. C.; Molinero, V.; Doherty, M. F.; Peters, B. *J. Am. Chem. Soc.* **2012**, *134*, 19544–19547.

(5) Lupi, L.; Hudait, A.; Molinero, V. *J. Am. Chem. Soc.* **2014**, *136*, 3156–3164.

(6) Cox, S. J.; Kathmann, S. M.; Slater, B.; Michaelides, A. *J. Chem. Phys.* **2015**, *142*, 184705.

(7) Chandler, D. *J. Chem. Phys.* **1978**, *68*, 2959–2970.

(8) Grote, R. F.; Hynes, J. T. *J. Chem. Phys.* **1980**, *73*, 2715–2732.

(9) Pollak, E. *J. Chem. Phys.* **1986**, *85*, 865–867.

(10) Garrett, B.; Schenter, G. *Int. Rev. Phys. Chem.* **1994**, *13*, 263–289.

(11) Haynes, G. R.; Voth, G. A.; Pollak, E. *Chem. Phys. Lett.* **1993**, *207*, 309 – 316.

(12) Haynes, G. R.; Voth, G. A.; Pollak, E. *J. Chem. Phys.* **1994**, *101*, 7811–7822.

(13) Haynes, G. R.; Voth, G. A. *J. Chem. Phys.* **1995**, *103*, 10176–10182.

(14) Schenter, G. K.; McRae, R. P.; Garrett, B. C. *J. Chem. Phys.* **1992**, *97*, 9116–9137.

(15) Truhlar, D. G.; Garrett, B. C. *J. Phys. Chem. B* **2000**, *104*, 1069–1072.

(16) Peters, B. *Chem. Phys. Lett.* **2012**, *554*, 248 – 253.

(17) Li, J.; Morrone, J. A.; Berne, B. J. *J. Phys. Chem. B* **2012**, *116*, 11537–11544.

(18) Pluharova, E.; Marsalek, O.; Schmidt, B.; Jungwirth, P. *J. Phys. Chem. Lett.* **2013**, *4*, 4177–4181.

(19) Fulton, J. L.; Schenter, G. K.; Baer, M. D.; Mundy, C. J.; Dang, L. X.; Balasubramanian, M. *J. Phys. Chem. B* **2010**, *114*, 12926–12937.

(20) Baer, M. D.; Pham, V.-T.; Fulton, J. L.; Schenter, G. K.; Balasubramanian, M.; Mundy, C. J. *J. Phys. Chem. Lett.* **2011**, *2*, 2650–2654.

(21) Fulton, J. L.; Bylaska, E. J.; Bogatko, S.; Balasubramanian, M.; Cauet, E.; Schenter, G. K.; Weare, J. H. *J. Phys. Chem. Lett.* **2012**, *3*, 2588–2593.

(22) Baer, M. D.; Fulton, J. L.; Balasubramanian, M.; Schenter, G. K.; Mundy, C. J. *J. Phys. Chem. B* **2014**, *18*, 7211–7220.

(23) Grimme, S. *J. Comput. Chem.* **2004**, *25*, 1463–1473.

(24) Baer, M. D.; Mundy, C. J.; McGrath, M. J.; Kuo, I. F. W.; Siepmann, J. I.; Tobias, D. J. *J. Chem. Phys.* **2011**, *135*.

(25) Dellago, C.; Bolhuis, P.; Geissler, P. *Advances in Chemical Physics, Vol 123*; Advances in Chemical Physics; 2002; Vol. 123; pp 1–78.

(26) Mullen, R. G.; Shea, J.-E.; Peters, B. *J. Chem. Theo. Comp.* **2014**, *10*, 659–667.

(27) Truhlar, D.; Isaacson, A.; Garrett, B. In *The Theory of Chemical Reaction Dynamics*; Baer, M., Ed.; The Theory of Chemical Reaction Dynamics; CRC Press, Boca Raton, Fl, 1985; Vol. 4; pp 65–137.

(28) Truhlar, D. G.; Garrett, B. C. *Acc. Chem. Res.* **1980**, *13*, 440–448.

(29) Becke, A. D. *Phys. Rev. A* **1988**, *38*, 3098–3100.

(30) Lee, C.; Yang, W.; Parr, R. G. *Phys. Rev. B* **1988**, *37*, 785–789.

(31) Dang, L. X.; Rice, J. E.; Caldwell, J.; Kollman, P. A. *J. Am. Chem. Soc.* **1991**, *113*, 2481–2486.

(32) Berendsen, H.; Grigera, J.; Straatsma, T. *J. Phys. Chem.* **1987**, *91*, 6269–6271.

(33) Jorgensen, W. L.; Maxwell, D. S.; Tirado-Rives, J. *J. Am. Chem. Soc.* **1996**, *118*, 11225–11236.

(34) Jorgensen, W. L.; Chandrasekhar, J.; Madura, J. D.; Impey, R. W.; Klein, M. L. *J. Chem. Phys.* **1983**, *79*, 926–935.

(35) van Erp, T. S. *ArXiv e-prints* **2011**,

(36) Essmann, U.; Perera, L.; Berkowitz, M. L.; Darden, T.; Lee, H.; Pedersen, L. G. *J. Chem. Phys.* **1995**, *103*, 8577–8593.

(37) Hess, B.; Kutzner, C.; van der Spoel, D.; Lindahl, E. *J. Chem. Theory Comput.* **2008**, *4*, 435–447.

(38) Bussi, G.; Donadio, D.; Parrinello, M. *J. Chem. Phys.* **2007**, *126*, 014101.

(39) Pluharova, E.; Baer, M. D.; Mundy, C. J.; Schmidt, B.; Jungwirth, P. *J. Phys. Chem. Lett.* **2014**, *5*, 2235–2240.

(40) Grossfield, A. WHAM: an implementation of the weighted histogram analysis method, version 2.0.2. http://membrane.urmc.rochester.edu/content/wham/.

(41) McRae, R. P.; Schenter, G. K.; Garrett, B. C.; Svetlicic, Z.; Truhlar, D. G. *J. Chem. Phys.* **2001**, *115*, 8460–8480.

(42) Isaacson, A. D.; Truhlar, D. G.; Rai, S. N.; Steckler, R.; Hancock, G. C.; Garrett, B. C.; Redmon, M. J. *Comp. Phys. Comm.* **1987**, *47*, 91 – 102.

(43) Smith, D.; Dang, L. *J. Chem. Phys.* **1994**, *100*, 3757–3766.

(44) Dang, L. X.; Annapureddy, H. V. R. *J. Chem. Phys.* **2013**, *139*.

(45) Remsing, R.; Rodgers, J.; Weeks, J. *J. Stat. Phys.* **2011**, *145*, 313–334.

(46) Geissler, P. L.; Dellago, C.; Chandler, D. *J. Phys. Chem. B* **1999**, *103*, 3706–3710.

(47) Peters, B.; Bell, A. T.; Chakraborty, A. *J. Chem. Phys.* **2004**, *121*, 4453–4460.

(48) Mullen, R. G.; Shea, J.-E.; Peters, B. *J. Chem. Phys.* **2014**, *140*, 041104.

(49) Schenter, G. K.; Garrett, B. C.; Truhlar, D. G. *J. Phys. Chem. B* **2001**, *105*, 9672–9685.

(50) Miller, W. H.; Handy, N. C.; Adams, J. E. *J. Chem. Phys.* **1980**, *72*, 99–112.

(51) Yonetani, Y. *J. Chem. Phys.* **2015**, *143*, 044506.

(52) Baer, M. D.; Mundy, C. J. *Faraday Discuss.* **2013**, *160*, 89–101.

(53) Remsing, R. C.; Baer, M. D.; Schenter, G. K.; Mundy, C. J.; Weeks, J. D. *J. Phys. Chem. Lett.* **2014**, *5*, 2767–2774.

(54) Sese, G.; Guardia, E.; Padro, J. A. *J. Phys. Chem.* **1995**, *99*, 12647–12654.